NAVAL POSTGRADUATE SCHOOL

MONTEREY, CALIFORNIA

THESIS

EXPERIMENTS IN PASSIVE SUPPRESSION OF LOW-FREQUENCY BROADBAND UNDERWATER SOUND

by

Richard L. Wyman III

December 2021

Thesis Advisor: Bruce C. Denardo
Co-Advisor: Oleg A. Godin

THIS PAGE INTENTIONALLY LEFT BLANK

REPORT DOCUMENTATION PAGE	*Form Approved OMB No. 0704-0188*

1. AGENCY USE ONLY *(Leave blank)*	**2. REPORT DATE** December 2021	**3. REPORT TYPE AND DATES COVERED** Master's thesis

4. TITLE AND SUBTITLE
EXPERIMENTS IN PASSIVE SUPPRESSION OF LOW-FREQUENCY BROADBAND UNDERWATER SOUND

5. FUNDING NUMBERS

6. AUTHOR(S) Richard L. Wyman III

7. PERFORMING ORGANIZATION NAME(S) AND ADDRESS(ES)
Naval Postgraduate School
Monterey, CA 93943-5000

8. PERFORMING ORGANIZATION REPORT NUMBER

9. SPONSORING / MONITORING AGENCY NAME(S) AND ADDRESS(ES)
N/A

10. SPONSORING / MONITORING AGENCY REPORT NUMBER

11. SUPPLEMENTARY NOTES The views expressed in this thesis are those of the author and do not reflect the official policy or position of the Department of Defense or the U.S. Government.

12a. DISTRIBUTION / AVAILABILITY STATEMENT
Approved for public release. Distribution is unlimited.

12b. DISTRIBUTION CODE
A

13. ABSTRACT (maximum 200 words)

A theoretical article by O. A. Godin and A. B. Baynes in 2018 predicts that an air-filled bladder near an underwater sound source can substantially suppress the sound emission. Practical applications include reducing the acoustic signature of naval vessels by placing a bladder near the propellers. We performed experiments in a Spanagel Hall tank and in Monterey Bay, comparing data to the theory. To improve previous thesis data gathered in the tank, we procured a more suitable sound source and a better bladder, and we increased the mass of the anchor that tethers the bladder, so that a larger bladder could be submerged. In addition, the method of gathering data was improved so that essentially continuous values occurred over our frequency range of 0.5 to 5.0 kHz. Data were gathered with and without the air bladder, and the ratio of the amplitudes were compared to predicted values, yielding positive trends. In Monterey Bay, an imploding lightbulb was used as a source while large balloons were used as a bladder. The bulb was burst at depth 10 meters with and without the balloons, and the sound was measured by a distant receiver. The data were compared to advanced theoretical models, accounting for some aspects of the environment. This initial attempt yielded encouraging results, indicating that the theory should be further tested by more controlled experiments in the ocean environment.

14. SUBJECT TERMS underwater sound suppression	**15. NUMBER OF PAGES** 65
	16. PRICE CODE

17. SECURITY CLASSIFICATION OF REPORT	**18. SECURITY CLASSIFICATION OF THIS PAGE**	**19. SECURITY CLASSIFICATION OF ABSTRACT**	**20. LIMITATION OF ABSTRACT**
Unclassified	Unclassified	Unclassified	UU

NSN 7540-01-280-5500

Standard Form 298 (Rev. 2-89)
Prescribed by ANSI Std. 239-18

THIS PAGE INTENTIONALLY LEFT BLANK

Approved for public release. Distribution is unlimited.

EXPERIMENTS IN PASSIVE SUPPRESSION OF LOW-FREQUENCY BROADBAND UNDERWATER SOUND

Richard L. Wyman
Ensign, United States Navy
BS, University of Maine, 2020

Submitted in partial fulfillment of the
requirements for the degree of

MASTER OF SCIENCE IN ENGINEERING ACOUSTICS

from the

NAVAL POSTGRADUATE SCHOOL
December 2021

Approved by: Bruce C. Denardo
Advisor

Oleg A. Godin
Co-Advisor

Oleg A. Godin
Chair, Department of Physics

THIS PAGE INTENTIONALLY LEFT BLANK

ABSTRACT

A theoretical article by O. A. Godin and A. B. Baynes in 2018 predicts that an air-filled bladder near an underwater sound source can substantially suppress the sound emission. Practical applications include reducing the acoustic signature of naval vessels by placing a bladder near the propellers. We performed experiments in a Spanagel Hall tank and in Monterey Bay, comparing data to the theory. To improve previous thesis data gathered in the tank, we procured a more suitable sound source and a better bladder, and we increased the mass of the anchor that tethers the bladder, so that a larger bladder could be submerged. In addition, the method of gathering data was improved so that essentially continuous values occurred over our frequency range of 0.5 to 5.0 kHz. Data were gathered with and without the air bladder, and the ratio of the amplitudes were compared to predicted values, yielding positive trends. In Monterey Bay, an imploding lightbulb was used as a source while large balloons were used as a bladder. The bulb was burst at depth 10 meters with and without the balloons, and the sound was measured by a distant receiver. The data were compared to advanced theoretical models, accounting for some aspects of the environment. This initial attempt yielded encouraging results, indicating that the theory should be further tested by more controlled experiments in the ocean environment.

THIS PAGE INTENTIONALLY LEFT BLANK

TABLE OF CONTENTS

THIS PAGE INTENTIONALLY LEFT BLANK

LIST OF FIGURES

LIST OF TABLES

THIS PAGE INTENTIONALLY LEFT BLANK

ACKNOWLEDGMENTS

First off, I would like to thank Koda Burger, my husky-Lab mix, for the concessions he had to make for the past year and a half as I spent many hours working on my thesis when they could have been spent going for a "W-word" or giving him belly rubs. I would also like to thank my girlfriend, Kaylee, for the same reasons (she LOVES going for a W-A-L-K).

In all seriousness, I would like to extend extraordinary thanks to Dr. Denardo. Not only was Dr. Denardo a valuable resource throughout the course of this undertaking, but he has also helped develop me into a better student, problem solver, and experimentalist. His countless hours in the lab and his reviewing of my work allowed progress to continue, especially in the not-too-uncommon scenario when I was unsure of how to proceed.

I also would like to thank Dr. Godin for all of his help in understanding and interpreting the complex yet intriguing theory he developed that allowed for this thesis to exist in the first place.

Additionally, I would like to thank Dr. Smith and Dr. Leary for their invaluable help in preparing for, conducting, and analyzing the experiments in the bay, despite their busy schedules. On the same note, I would like to thank the crew of the R/V Fulmar for allowing us to conduct the experiments as well as Mandy Shoemaker for taking pictures throughout the experiment.

I would like to thank Mr. Jay Adeff for all of his help, especially in helping us take quicker, more accessible data, which was invaluable.

Finally, I would like to thank all of my instructors and peers here at NPS for making the challenging past year and a half the best experience possible.

THIS PAGE INTENTIONALLY LEFT BLANK

I. INTRODUCTION

A. BACKGROUND

As underwater detection capabilities are continuously improving, anti-detection measures become increasingly important. A theory published by Godin and Baynes, "Passive, Broadband Suppression of Radiation of Low-Frequency Sound" lays the foundation for a method of limiting underwater detection [1]. The theory states that through the placement of an air-filled bladder near an underwater sound source, a broadband of low-frequency sound can be suppressed. The naval application of this theory is of particular interest, as placing a bladder, as described by Godin and Baynes, near the propeller of a naval vessel could decrease the acoustic signature and therefore the probability of detection. Furthermore, the reduction of self-noise could serve to improve detection capabilities of naval vessels. There is also benefit to be gained from the application of this theory to commercial vessels, thereby lowering noise in discrete cases and throughout the world's oceans.

Before any practical application is feasible, a proof-of-concept is necessary in order to allow for more research efforts to be focused on the project. In this thesis, we worked as a follow-up and continuation of an NPS thesis by Evan McMellon [2] to compare experimental results to the theory. In McMellon's thesis, a promising trend was discovered but due to the hurdles and limitations of the experiment, more research was required to determine agreement between the theory and experimental data.

In this thesis we improve upon the experiments conducted in the previous thesis by using a more suitable sound source (Section II.A), improving the air-filled bladder, increasing the number of data points taken (Section II.D), and by testing in more suitable environments. The experiment was conducted in the tank lab of Spanagel Hall (Chapter II) in a manner similar to that of the previous thesis. Sets of data were taken over a frequency range of 0.5 to 5 kHz both with and without a nearby air bladder and compared to the theoretical model. Furthermore, to provide the most practical proof of concept, an experiment was conducted in Monterey Bay (Chapter III).

B. THEORY

The Godin and Baynes article "Passive, Broadband Suppression of Radiation of Low-Frequency Sound" details the suppression of sound from a source in close proximity to a soft sphere [1]. Figure 1 depicts the geometry relevant to the theory of suppression and our experiments.

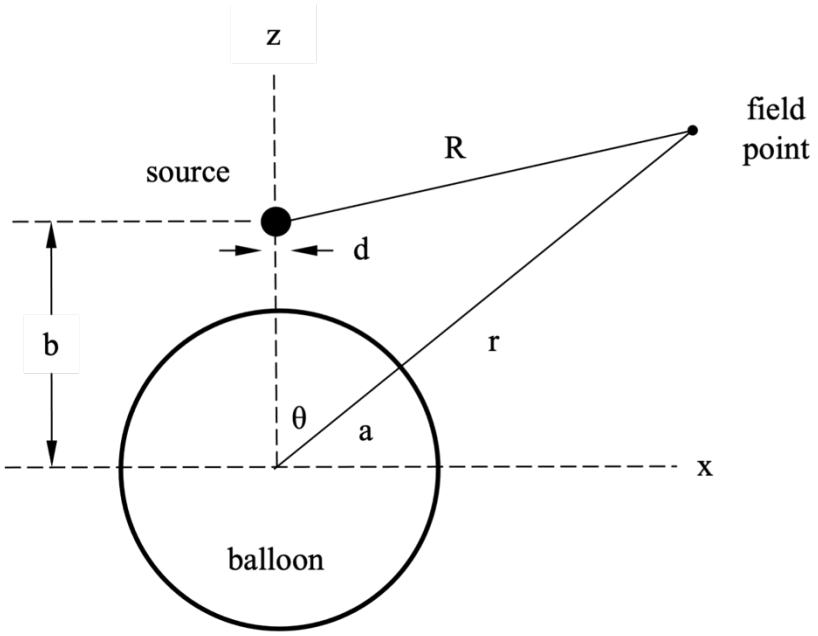

Figure 1. Geometry of source, receiver, and sphere, as presented by theory

In this geometry, the sphere is of radius a, with a distance from the center of the sphere to the center of source b so that b-$a > 0$. The quantity R is the distance from the center of the source to the center of the receiver while r is the distance between the center of the sphere and the center of the receiver. The quantity M is taken as the ratio of the density of the sphere and the density of water. In our practical modeling, this was primarily taken as the ratio of the densities of air and water. Similarly, s is the ratio of the speed of sound in the medium of the sphere and the speed of sound in water. Likewise, this value is most often computed in our modeling as the ratio of the speed of sounds in air and water. Lastly, θ is defined as the angle between the centerline of the source and sphere and the

line of the center of the sphere and the receiver. In our controlled tank experiments, we found that it is easiest to align to a θ of zero.

The pressure amplitude of the spherical radiation pattern with no sphere is given by

$$P_{sph} = \frac{D}{R}, \tag{1}$$

in which D has units of Pa·m. The Godin and Baynes theory derives the pressure amplitude in the presence of a soft sphere as

$$P = kD|\sum_{n=0}^{\infty}(2n+1)P_n(cos\,\theta)\,h_n(kr)[j_n(kb) - A_n h_n(kb)]|. \tag{2}$$

In this equation, $k=\omega/c=2\pi f/c$ for frequency, f and sound speed in water, c. P_n represents Legendre polynomials, j_n represents spherical Bessel functions of the first kind, and h_n represents spherical Hankel functions of the first kind. For an idealized sphere in which M approaches zero—indicating a negligible density—the value A_n can be given by

$$A_n^{(S)} = \frac{j_n(ka)}{h_n(ka)}. \tag{3}$$

For the more realistic case where the sphere is filled with a fluid with a density and speed of sound greater than zero, the value A_n becomes

$$A_n^{(F)} = \frac{Msj_n'(ka)j_n\left(\frac{ka}{s}\right) - j_n(ka)j_n'\left(\frac{ka}{s}\right)}{Msh_n'(ka)j_n\left(\frac{ka}{s}\right) - sh_n(ka)j_n'\left(\frac{ka}{s}\right)}. \tag{4}$$

The derivative of the spherical Bessel and Hankel functions is given by

$$g_n'(x) = \frac{n}{x}g_n(x) - g_{n+1}(x), \tag{5}$$

in which g_n is equal to either j_n or h_n.

Through the combination of Equation (1) and Equation (2), the pressure ratio with and without a nearby sphere can be calculated as

$$\frac{P}{P_{sph}} = e^{-ikR}kR|\sum_{n=0}^{\infty}(2n+1)P_n(cos\,\theta)\,h_n(kr)[j_n(kb) - A_n h_n(kb)]|. \tag{6}$$

It is important to note that the effect is generally most obvious over low frequencies, specifically in the following regime:

$$d \ll b - a \ll a \ll \lambda. \tag{7}$$

Furthermore, as the radius of the sphere increases, the pressure ratio tends to decrease, indicating a greater suppression. Similarly, as the distance between the source and the sphere decreases, the pressure ratio typically decreases. Through application of the theoretical equations, it is apparent that slight increases in the sound speed in water also could improve the suppression of sound, although not significantly. As expected, the same can be said for range, as the further the receiver is, it is typical that the pressure ratio is lesser. An increase in *M* is commonly detrimental to suppression, indicating that the lesser the density of the sphere, the better suppression will be.

II. EXPERIMENTS IN SPANAGEL HALL TANK

A. SEARCH FOR UNDERWATER SOURCE

In McMellon's thesis [2], one of the areas that required improvement was the source—in McMellon's thesis, a hydrophone was used. One problem was that the amplitude of the source could drift, despite there being a constant drive voltage amplitude. In reference to specifications in the theory (Section I.B), optimal conditions for suppression occur when the diameter of the source, *d*, is significantly less than the radius of the sphere, *a* [1]. Due to the nature of the tank experiment, the radius and therefore volume of the sphere was limited by the weight of the anchoring system (Section II.C). Keeping this constraint in mind, it became necessary to find the smallest possible source that still allowed for sufficiently high amplitude sound to be transmitted without being overdriven. The source also needed to project this amplitude at low frequencies, as the suppression effect is easiest to measure when projecting at higher amplitudes. Finally, it was advantageous to search for an omni-directional, spherical source, as is assumed in the theory.

A number of sources were considered in order to improve the experimental process, including the continued use of a hydrophone as well as alternate sources. Physical means of creating higher amplitude sound were considered in utilizing an imploding lightbulb as well as striking a metal plate. It was decided that these options, while viable for future testing, could likely present more problems than the use of a hydrophone in the tank environment. It was also considered that in using these methods with the possible sphere sizes, the distance *b-a* would be much larger than when using a traditional projector. Other potential sources included projectors from CeramTec, Piezo Kinetics, and Data Physics. After submitting queries with each of the companies, it was determined that the CeramTec and Piezo Kinetics options did not include spherical projectors [3], [4]. The sources offered by Data Physics were determined to be significantly larger than what would be suitable for the tank experiments [5]. Another option that was considered was using an acoustic modem, which is used to transmit data underwater. Upon further review, it was determined that it would be difficult to find an acoustic modem that was small enough and viable within

the low frequency range needed for the experiment [6]. The International Transducer Corporation (ITC – now a part of Gavial) offered a series of projectors that were both spherical, small, and operated at the necessary low-frequency ranges.

After further inquiry, the ITC-1042 was deemed to be the most suitable source available. The ITC-1042 is a spherical transducer that can act both as a transmitter and receiver [7]. It has a diameter of 1.4 inches, making it much smaller than the 2.7 inch source used in McMellon's experiments [2]. The transducer has a suggested frequency band of 0.01 – 100 kHz, which allows for operation in our experimental frequency range of 0.5 – 5 kHz [7].

B. MAXIMUM DRIVE AMPLITUDE FOR ITC-1042

The ITC-1042 transducer (Section II.A) has the maximum electrical input power Π_{max} = 100 W. Exceeding this value could damage the transducer. The purpose of this section is to determine the maximum input voltage as a function of frequency. The voltage was determined from laboratory measurements with an impedance analyzer.

In general, the electrical input power is $\Pi = \langle Re(V)Re(I) \rangle$, where V is the instantaneous complex voltage and I is the instantaneous complex current, and where the brackets denote a time average. We are free to assume that V is real, but I must be complex in order to account for a phase difference. The power is then $\Pi = \langle VRe(I) \rangle$. The current is $I = YV$, where Y is the complex input admittance, which is the reciprocal of the impedance [8]. The admittance is expressed as $Y = G + iB$, where the real part is the conductance G, and the imaginary part is the susceptance B. The power is then $\Pi = GV_0 2$, where V_0 is the rms voltage amplitude. To determine the maximum voltage, we set the power equal to the maximum value. The result is that, by measuring G as a function of frequency, we can determine the maximum rms amplitude of the input voltage as a function of frequency:

$$(V_0)_{max} = \sqrt[2]{\frac{\Pi_{max}}{G}}, \tag{8}$$

where Π_{max} = 100 W for the ITC-1042. Ideally, the measurements should be performed *in situ*, with the same arrangement as the noise suppression experiment both with and without

the balloon. The effect of unwanted but probably unavoidable reflections off surfaces will then be included. However, we only require approximate values of $(V_0)_{max}$, so admittance measurements in another tank should be sufficient, as long as the tank is not too small.

In our ultimate goal of experimentally observing acoustic suppression, only low underwater frequencies are relevant, which lie approximately in the decade of 0.5 to 5 kHz. By comparison, the resonance frequency of the ITC-1042 is 79 kHz. The electrical side of the transducer is essentially a capacitance C_0, which has admittance $i\omega C_0$. For low frequencies, the admittance is then expected to be relatively small, and so the maximum voltage amplitude is expected to be relatively large. It could easily be in the kilovolt range, which means that we would have to use a transformer if we need to obtain the maximum possible acoustic amplitude. However, in a previous thesis [2], it was found that the use of a transformer can be problematic in several ways. Having to use a transformer depended upon the acoustical signal-to-noise ratio, which we determined by experiment. However, it was important to recognize that the maximum voltage amplitude (8) had to first be determined so that we could avoid any damage to the transducer.

A graph of admittance measurements of the ITC-1042 is supplied by the manufacturer. Unfortunately, the frequency range of the graph begins at 10 kHz, which is above our range, and the scale of the values of G is such that the value at 10 kHz is imperceptibly different from zero. At 30 kHz, the value is approximately G = 100 μmho = 100 x 10–6/Ω, which is the smallest increment of the scale. This value is a rough upper bound for our experiment. A more accurate value is greater by very roughly an order of magnitude. The maximum rms voltage (8) corresponding to the G value at 30 kHz, where Π_{max} = 100 W, is

$$(V_0)_{max} = \sqrt[2]{\frac{100}{100\times10^{-6}}} = 1.0\ kV, \tag{9}$$

where all units in the calculation are SI. Again, we emphasize that a more accurate value of the maximum rms voltage is greater by very roughly an order of magnitude.

In conclusion, because $(V_0)_{max}$ in Equation (9) is in the kilovolt range, we could perform experiments in the range of hundreds of volts without damaging the transducer. In

the future, if a transformer or a higher-voltage amplifier is used, measurements of the conductance, *G*, of the ITC-1042 will yield the maximum allowable voltage.

C. IMPROVEMENTS TO ANCHORING SYSTEM

Due to the buoyant force on the compliant sphere, an anchor is required to keep the sphere underwater. Bolting a pulley to the bottom of a large tank would have been very difficult, unless the tank was temporarily drained. In our initial experiments, we used the original anchor [2], which consisted of two lead bricks sandwiched between two parallel plates held together with bolts. The bricks were prevented from sliding by shallow milled sections of the plates. Four of the bolts provided the legs that rested upon bottom of the tank. The legs were required due to the absorber on the bottom of the tank. Four other bolts had eyelets that were connected to cords that were used to lower and raise the anchor. The pulley that was used in submerging the sphere was connected to a ninth eyelet bolt in the center of the anchor.

We found that the anchor was not sufficiently heavy to suspend spheres even only slightly larger than previous ones (approximately 9 inches in diameter). The anchor moved in these cases. We thus decided to add two more lead bricks, especially due to prospective future research in a larger tank. The adding of the two bricks was accomplished by rotating the bricks by 90 degrees along their lengths to allow the plates to hold all four bricks. For the assembly to be sufficiently strong and remain submerged for long periods of time, we redesigned and replaced all of the hardware with stainless steel 5/16-inch threaded rod and nuts, as well as larger stainless steel eyebolts (Figure 2). We used a new pulley that was the same type as used by McMellon [2]. This pulley is *not* made of stainless steel and should be replaced with a stainless steel one for future research.

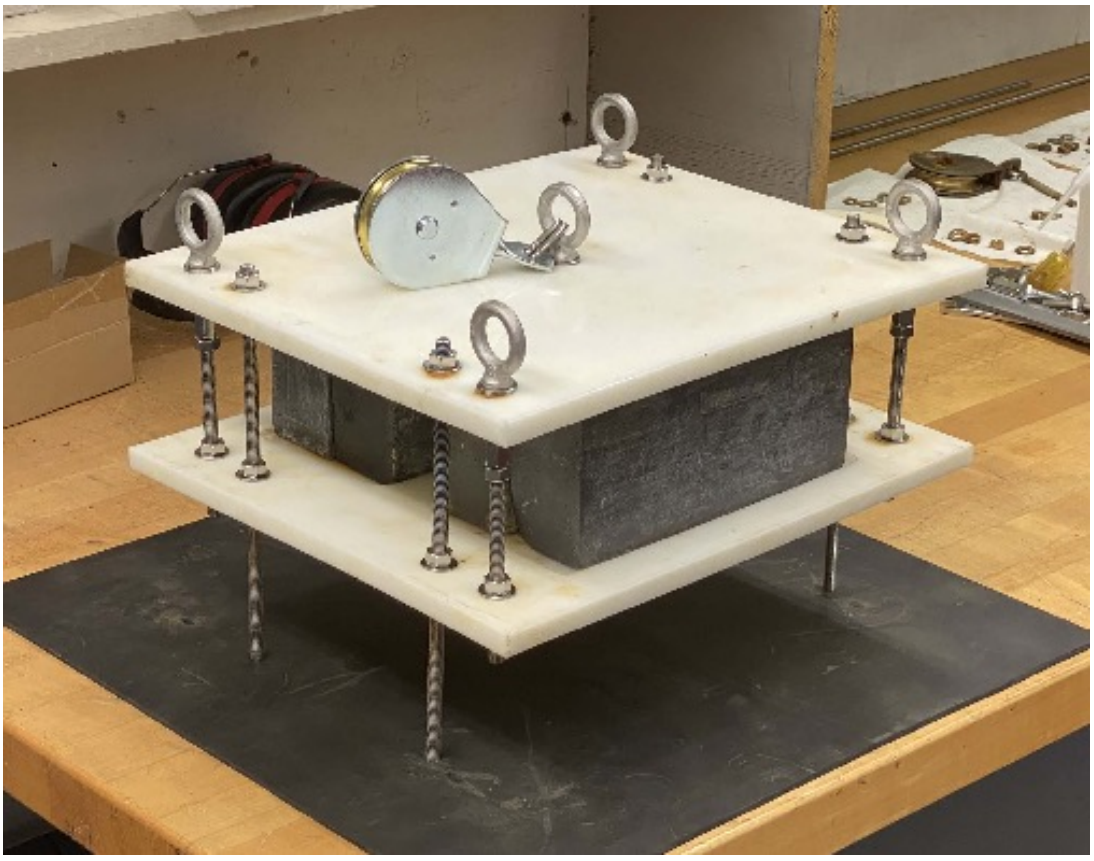

Figure 2. Anchor that holds a compliant sphere

To be able to perform experiments with larger compliant spheres in order to obtain greater sound suppression, we now calculate the maximum force that the anchor can support. Each of the four lead bricks has dimensions 2 in x 4 in x 8 in, and weighs 27 lbs (in air). Each of the two plates has dimensions 14 in x 12 in x 1/2 in. The weight of the anchor in air is measured to be W = 115 lbs. The weight is dominated by the lead bricks which weigh a total of 27 x 4 = 108 lbs.

By Archimedes' law, the buoyant force on a body of volume V is

$$F_B = \rho g V, \tag{10}$$

where the density of water is ρ = 1.00 x 103 kg/m3 and the acceleration due to gravity is g = 9.8 m/s^2.

The total volume of the anchor is approximately the volume of the bricks and plates, which is $V = 4(2 \text{ x } 4 \text{ x } 8) + 2(14 \text{ x } 12 \text{ x } 1/2) = 256 + 168 = 424 \text{ in}^3 \text{ x } (0.0254 \text{ m} / 1 \text{ in})^3 = 6.95 \text{ x } 10^{-3} \text{ m}^3$. The buoyant force on the anchor is then

$$F_{anchor} = \rho g V = (1.00 \times 10^3) \times 9.8 \times (6.95 \times 10^{-3}) = 68.1\ N = 15.3\ lbs. \quad (11)$$

The anchor can then support the maximum vertical force

$$F_{max} = W - F_{anchor} = 115 - 15.3 = 100\ lbs. \quad (12)$$

However, it is important to recognize that this value does *not* equal the maximum buoyant force on a sphere. The reason is that the pulley causes *two* tension forces to be exerted on the anchor. The arrangement is shown in Figure 3.

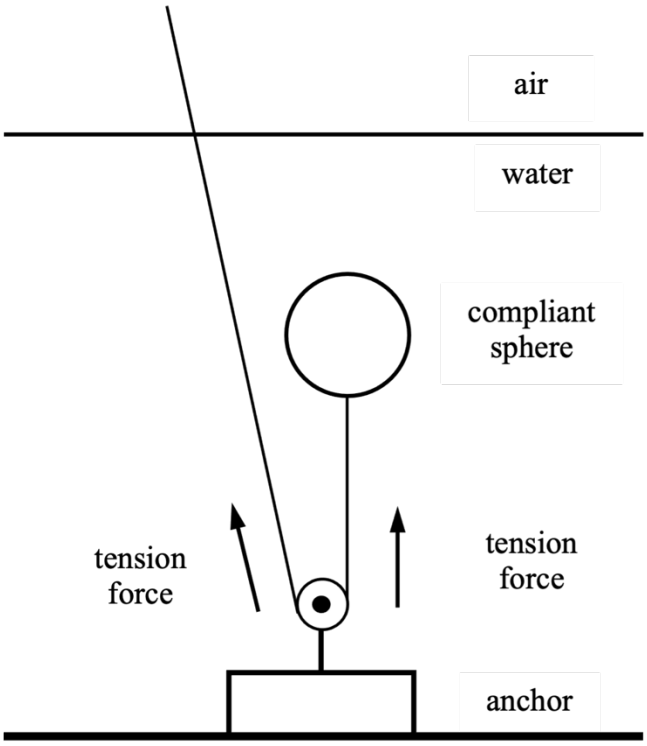

Figure 3. Geometry of the experimental setup (not to scale)

Since one segment of the chord is not vertical, the maximum tension T_{max} of the cord is somewhat less than $F_{max}/2$. To have a margin of error in our calculation, we assume that $T_{max} = F_{max}/2$, which has the value

$$T_{max} = 50\ lbs = 222\ N. \tag{13}$$

The buoyant force on a sphere of diameter D is

$$F_{sphere} = \rho g V_{sphere} = \frac{1}{6}\pi\rho g D^3. \tag{14}$$

Setting $F_{sphere} = T_{max}$, and solving for D, yields the maximum diameter

$$D_{max} = \left(\frac{6T_{max}}{\pi\rho g}\right)^{1/3} = \left(\frac{6\times222}{\pi\times10^3\times9.8}\right)^{1/3} = 0.351\ m = 13.8\ in. \tag{15}$$

There was a remaining problem that only became apparent when we experimented with the modified anchor. The nonvertical section of the cord in Figure 3 introduces a horizontal component of the force on the anchor. The vertical component reduces the normal force of the bottom of the tank on the anchor. The result was that the anchor moved, which was inconvenient because the anchor then needed to be repositioned. The submerging of a sphere had to be done slowly and carefully to avoid this motion.

D. METHOD OF DATA COLLECTION

1. Tow Tank

As in McMellon's thesis, we conducted the tank experiments in the furthermost tank in the basement of Spanagel Hall (Sp-025). The tank has the following dimensions: 21 feet in length, 7 feet in width, and a water depth of 7 feet and 4 inches. The tank is lined with a rubber anechoic material along the walls and its floor; however, the material is most effective at frequencies greater than 10 kHz, which is well above the frequency range that we were testing in. Due to this, it is not expected that the anechoic material significantly dampened any reflections off of the surfaces of the tank [2].

2. Air Bladder

The best material to use for the bladder was determined to be a punch balloon. A punch balloon is a toy consisting of a balloon attached to a rubber band (which we removed for our experiments). After experimentation with several different bladders, the punch balloon was determined to allow for the maximum value of the radius, *a,* while also having the best combination of durability, sphericity, and density. During experimentation, standard balloons were used, although it was found that they were often not durable and were also quite oblong. Additionally, beach balls were used but the material was determined to be too dense, as the theory indicates that a lesser areal density allows for better suppression. A punch balloon of equatorial diameter 12.5 inches is shown in Figure 4.

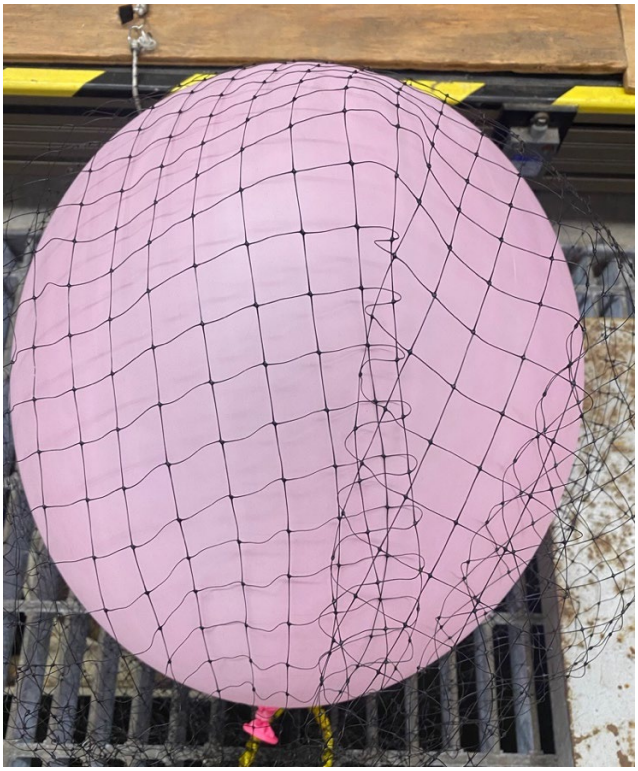

Figure 4. Punch balloon in netting

To secure the balloon to the anchoring system (Section II.C), a netting was placed around the balloon, as shown in Figure 4. The netting allowed for the pressure due to the buoyancy force to be dispersed throughout the surface of the balloon while also allowing

it to hold its shape to a degree. Once the balloon was inside the netting, a line was sinched, ensuring the balloon remained in position.

The measurement of the balloon radius is integral to the comparison to the theoretical predictions. The maximum diameter of the brand of punch balloon used was 18 inches [9]. However, due to buoyancy constraints determined by the weight of the anchor (Section II.C), the actual maximum diameter had to be much smaller. This allowed for increased durability in the balloons as they would be well below their maximum pressure. Since the balloons were not perfectly spherical, two measurements had to be taken in order to determine the dimensions of the balloon. The first measurement was the equatorial diameter – taken at the widest point between the crest of the balloon and the tie off point. The second was the longitudinal diameter – taken from the crest of the balloon to the tie off point. It was desirable to determine the effective radius in order to properly compare the sphere to the theoretical models. The effective radius was taken as the radius that a perfect sphere of the same volume as our balloon, an ellipsoid, would have. To calculate the effective radius, a, the geometric mean was calculated using the equatorial diameter twice and the longitudinal once as show in Equation (16):

$$a = \frac{1}{2}\left(D_{Equatorial}^{2} * D_{Longitudinal}\right)^{1/3}. \tag{16}$$

3. Geometry

Figure 5 shows the rough geometry used in the tank lab experiments. For reference, the tank is seven feet wide with the source, anchor, and balloon in the foreground and the receiver in the background of Figure 5. The source and the anchor were placed in the same section of the tank, with the source being lowered to the halfway between the bottom and the surface of the water in the tank: three feet, eight inches. Farther along the tank, just over two meters, the receiver was aligned and lowered to the same point in the water. The balloon would attach to the anchor and carefully be lowered to half the depth of the tank, just behind the source.

Figure 5. Geometry of the tow tank set-up

4. Equipment

The source used in the tank experiments was an ITC-1042 reversible transducer (Section II.A). The source was driven at 120 V_{rms}, which is near the maximum value for our amplifier. The receiver used in the experiments was a Bruel and Kjaer (B&K) 8103 hydrophone, the same as was used in McMellon's thesis [2].

In order to store the necessary equipment for the experiments, an equipment rack was used, shown in Figure 6. We used a QSC MX1500a Professional Stereo Amplifier to

drive the transducer. In order to amplify and filter the received signal, we used a Stanford Research SR560 Pre-Amplifier with a gain of 103 and a bandpass filter of 100 Hz – 10 kHz. In order to monitor the voltage across the transducer to watch for drifting, we used a Hewlett Packard HP34401A Multimeter. Additionally, we used a Stanford Research SR785 Signal Analyzer in order to record our received data and transfer the output into a computer accessible file.

The SR785 Signal Analyzer allowed us to transition from the method of taking discrete data points at quarter or half kilohertz intervals to using the swept sine function to take essentially continuous data along the entire frequency range from 500 Hz to 5 kHz. We compared the results of the swept sine when adjusting the number of data points taken. We concluded that 1024 was an adequate number as the resolution did not improve noticeably for our frequency range when increasing from 1024 to 2047. Additionally, we determined that having 20 integration points and 20 settle cycles was adequate as the output did not change in any significant manner.

Figure 6. Equipment stack used in tank experiments

5. Experimental Procedure

The experimental procedure in the tank lab experiments was quite simple. First, we would carefully record all necessary measurements: balloon diameter/radius (a), distance from source to balloon (b-a-$d/2$), and distance from source to receiver (R). Next, we would slowly and carefully submerge the balloon (in netting) so that the center of the balloon was aligned with the transducer, ensuring that the balloon is not moving. Next, we would drive the transducer and begin the swept sine measurements, ensuring to export the trace when

complete. We would then take another set of data with the balloon immediately after. We would then remove the balloon and take two more sets of data without the balloon in the same manner. Finally, we would compare the two sets of data taken (with-with or without-without) in order to verify short term reproducibility and accuracy in the results, which had been an issue in previous experiments.

E. EXPERIMENTAL DATA AND COMPARISON TO THEORY

After refinement of the experimental procedure, a final data set was taken with the specifications presented in Table 1. The data were taken in accordance with the experimental procedure outlined in Section II.D.5.

Table 1. Experimental parameters

$D_{equatorial}$	$D_{longitudinal}$	a	b-a-$d/2$	b	R
12.5 in	14.75 in	6.6 in	0.75 in	8.05 in	2.24 m

The received voltage with and without the presence of the balloon is shown in Figure 7 (created using MATLAB 2021a, as all plots in this thesis were) [10]. A very clear trend can be seen as the voltage for the trial with the balloon was less than that without the balloon on average throughout the frequency range. It is important to note that this trend is even more apparent for the lower end of the frequency spectrum. Specifically, the effect is shown to be most prominent at frequencies less than 3 kHz. Also, important to note is that there is even an amplification of the pressure level indicated as the voltage with the balloon is greater than that without at certain points in the higher end of the frequency range (above 4 kHz).

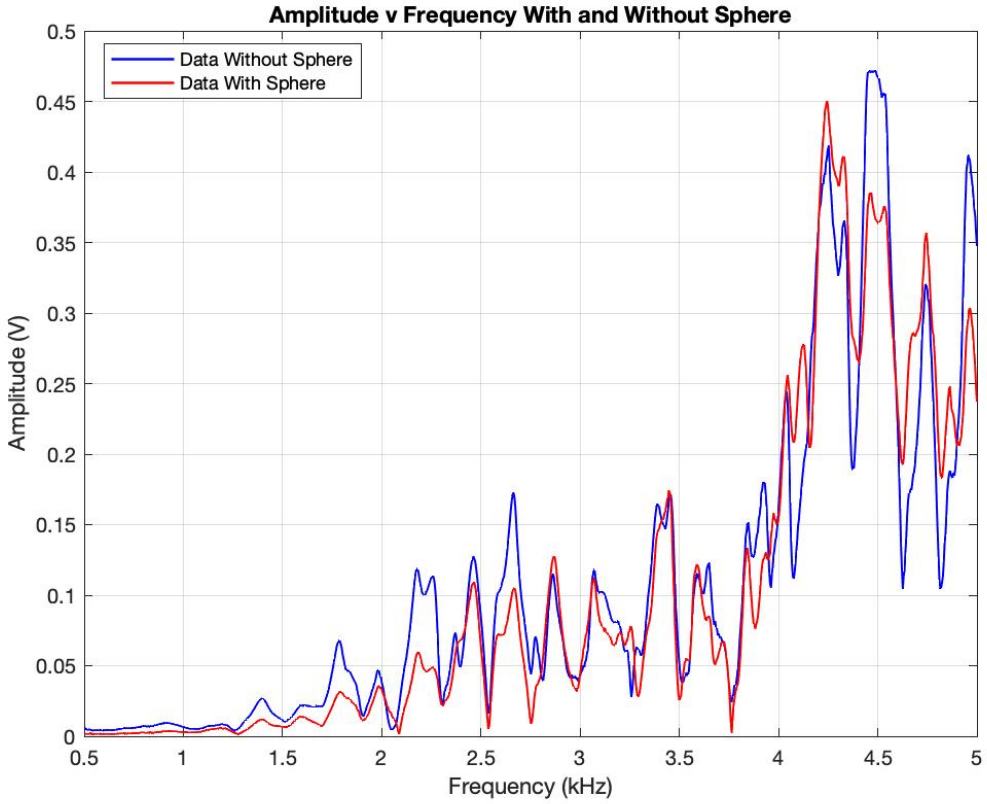

Figure 7. Comparison of raw data with and without sphere

To compare the experimental data to the theory, theoretical models were generated using the recorded values in Table 1 as well as reasonable estimates for the remaining theoretical parameters discussed in Section I.B [1]. All theoretical models given in this thesis were generated using Wolfram Mathematica [11]. These parameters are shown in Table 2. The theoretical model allowed for the pressure ratio with and without a sphere to be plotted over our experimental frequency range. The experimental pressure ratio was then calculated by dividing the received voltage with the balloon by the voltage without the balloon. The comparison of the experimental and theoretical pressure ratios are shown in Figure 8.

Table 2. Theoretical parameters (without dissipation)

c	*a*	*b*	*R*	*M*	*S*
1450 m/s	0.16 m	0.19 m	2.21 m	0.001225	2/9

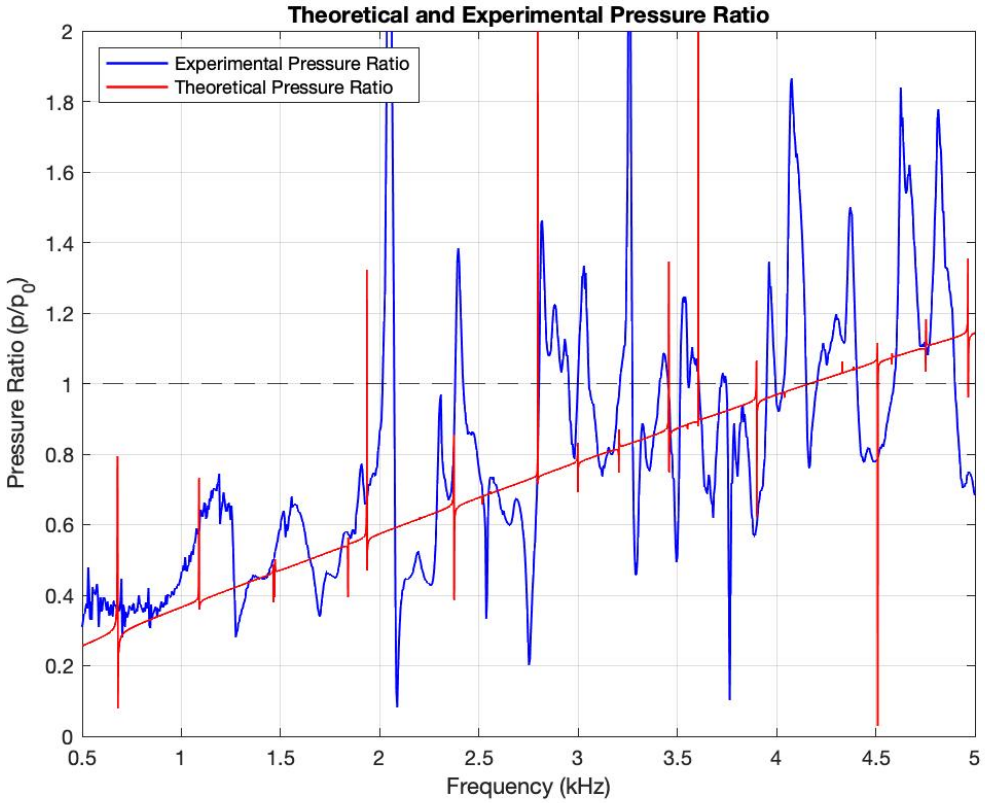

Figure 8. Comparison of experimental and theoretical pressure ratios (without dissipation)

The plot of the experimental and theoretical pressure ratio (Figure 8) indicates a general agreement between the theory and the experimental data. In many cases, the resonances seem to be in relative agreement as well as the general trend. However, this effect can be misleading and bring about the appearance of more alignment between theory and results as there truthfully is. The theoretical curve presented in Figure 8 does not account for dissipation inside the sphere, which affects the resonances shown in the plot. In order to correct this and create a more accurate model, dissipation was accounted for in the model by slightly altering the value of *s*. The input for *s* was changed from simply 2/9

to the complex value of 2/9(1+0.01i), producing the more realistic theoretical curve given in Figure 9.

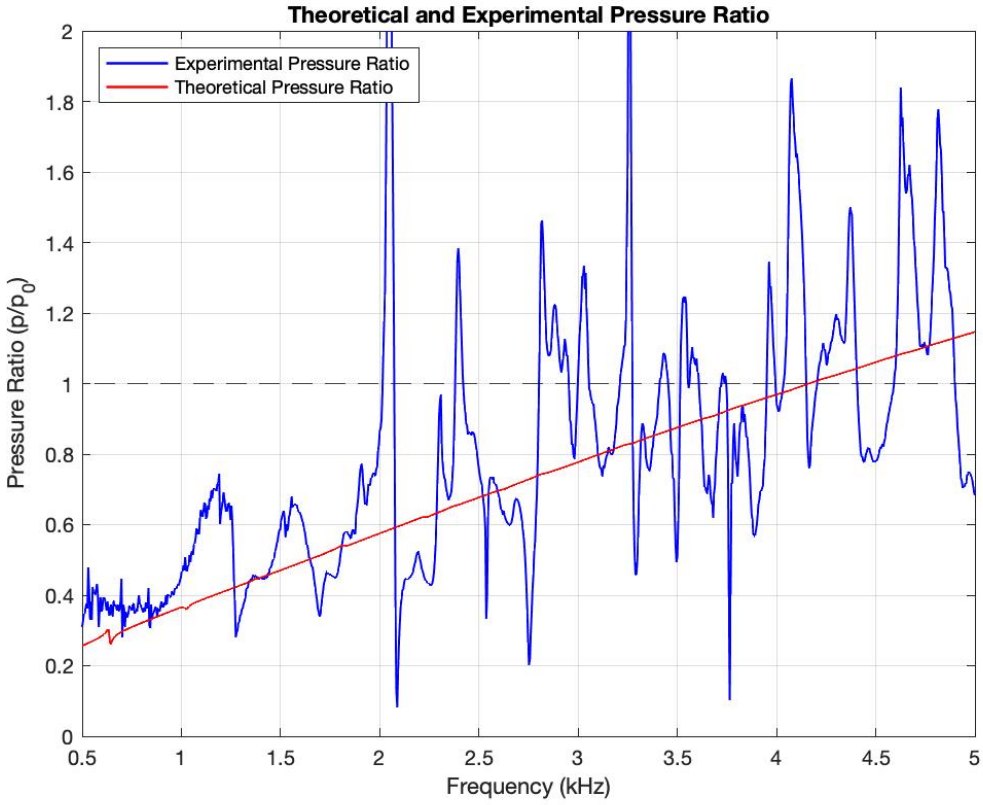

Figure 9. Comparison of experimental and theoretical pressure ratios (dissipation included)

The updated theoretical prediction shows much less agreement with the experimental results over the given frequency range due to the relative absence of resonances in the theory. The relative disappearance of resonances leads us to believe that the resonances depicted in the experimental data are not the result of the sphere, but more likely the result of tank resonances and reflections. It should be noted that the anechoic absorber in the tank is only effective at frequencies greater than 10 kHz, meaning reflections are still very significant in this experiment. Further supporting this is that the theoretical model used assumes an open space, which is clearly not present in the confines

of the Spanagel Hall tow tank (Section II.D.1). Based upon such clear differences between the theoretical model and the experiment, it was not expected that the two would agree completely, but rather that there would be a general sense of similarity.

In order to better compare the data without interference from the resonances in the experimental data, a moving average was applied to the experimental data and compared to the theoretical curve, shown in Figure 10. The moving average was calculated by first squaring the pressure amplitude values to work in units of intensity. Once converted to intensity, the moving average was taken, and the averaged data was converted back to units of pressure.

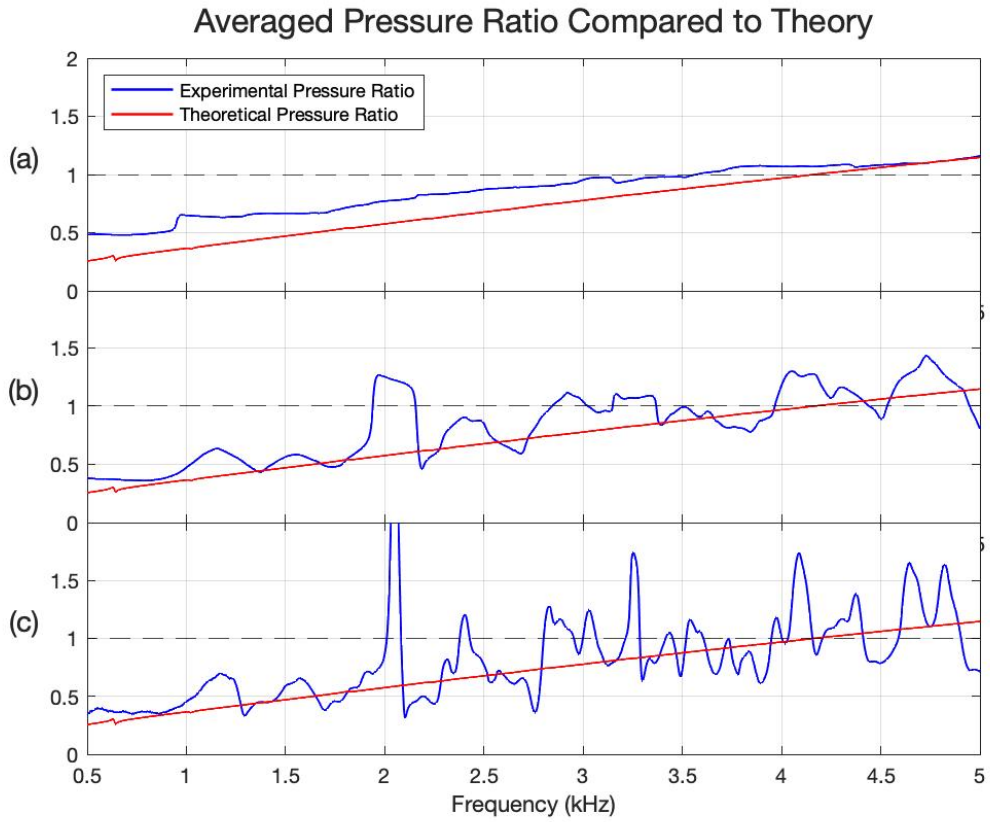

Figure 10. Pressure ratio compared to theory averaged using a moving average of (a) 500 points (2150 Hz) (b) 50 points (215 Hz) and (c) 10 points (43 Hz)

As the experimental data is smoothed, the most basic trend of the data becomes clearer and more easily comparable to the theoretical curve. There is a degree of agreement between the theoretical and experimental curves. However, due to the limitations of the tank environment, we cannot have significant conviction in any conclusions drawn from the results. Again, it is important to consider that the assumptions of the theoretical model and the parameters of the experiment differ significantly, meaning that any indication of agreement is still very promising. It is worth noting, that as the band used in averaging increases, the interference due to the reflections show to be above the theoretical values. Based on this, it can be reasonably concluded that the most significant of the differences between experimental values and theory can be attributed to the reflections from the surfaces of the tank.

III. EXPERIMENTS IN MONTEREY BAY

A. METHOD OF DATA COLLECTION

1. Overview

An initial proof-of-concept experiment was conducted to test the sound suppression theory in a practical environment. The R/V Fulmar was available to allow testing on August 12, 2021, in Monterey Bay. The experiment was intended to be simple and provide a rough estimate of the results of the implementation of the theory in an ocean environment. An imploding lightbulb was used as the source and a bottom-mounted, distant receiver was used. The planned geometry of the source, sphere, and weights experiment is included in Figure 11. The arrangement includes the source being suspended by a line to the desired depth while the air bladder is attached to the same line and weighted down by weighted bags.

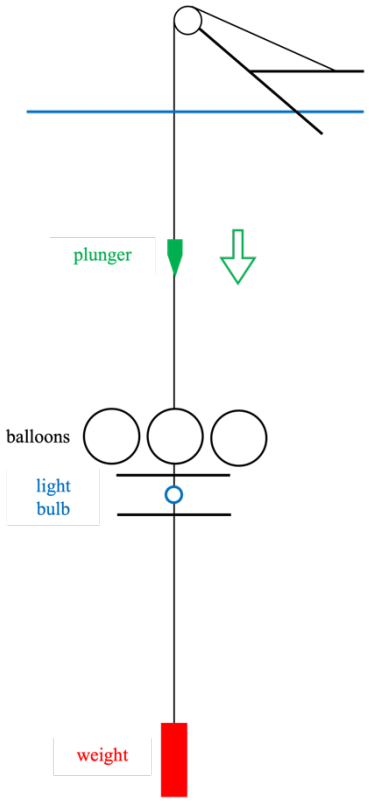

Figure 11. Planned experimental set-up

2. Apparatus

For the air bladder, balloons with a maximum diameter of 18 inches were used. Four balloons were filled to roughly 16 inches in diameter the day before the experiment and were placed in a larger plastic bag inside of a burlap sack in order to protect the balloons. The four balloons previously filled burst before the experiment, leading to two additional balloons being filled the day of the experiment. These balloons were inflated to a lesser diameter which was unable to be accurately measured but is approximated to be between 12 and 14 inches. The two balloons were both placed side by side and wrapped by the plastic bag and placed inside of the burlap bag for protection. The burlap bag was then tied off on a line in order to ensure a close proximity of the balloons to the source. It is important to note that the addition of the plastic bag and the burlap increase the density of the air bladder, therefore increasing the theoretical parameter, *M*. The experimental set up is shown in Figure 12.

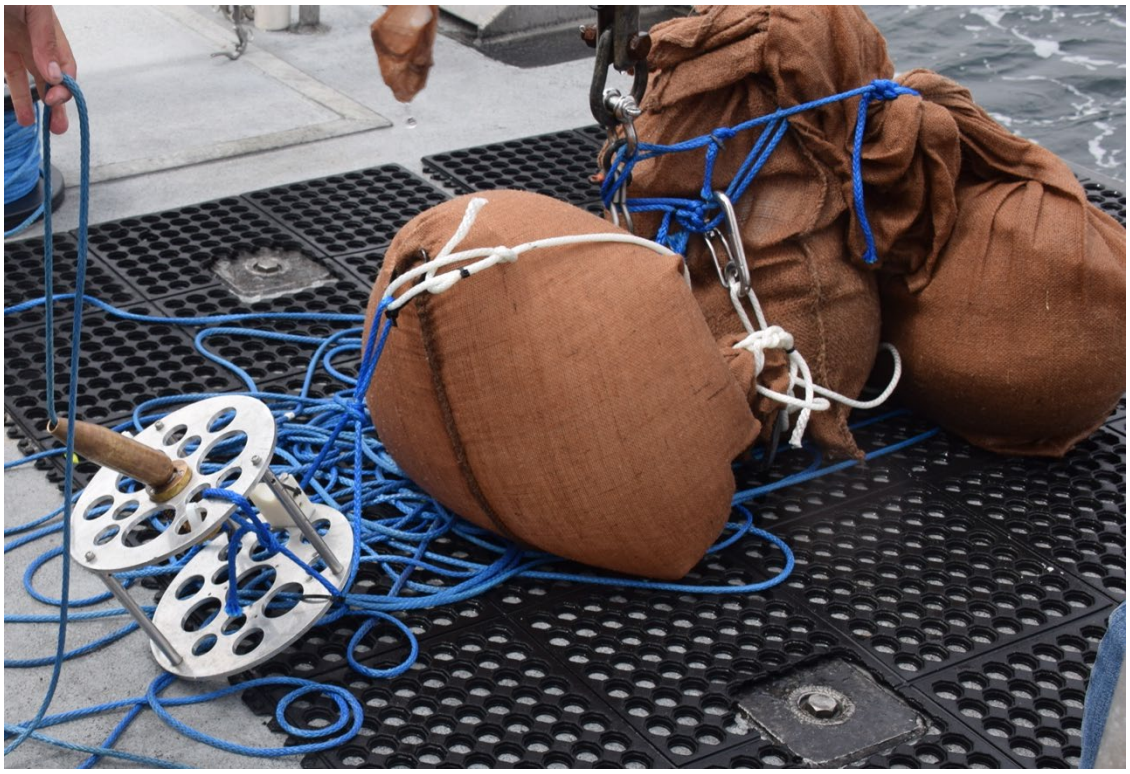

Figure 12. Experimental set-up in Monterey Bay experiments

Figure 12 shows the source, the air bladder, and the weighting system. The source, shown in the left of Figure 12 consists of a round, roughly five inch diameter lightbulb, which was wrapped in pantyhose and placed into the apparatus. The lightbulb was held in place and the enclosure was tied off onto the line. As the line was submerged, the plunger, shown above the metal apparatus in Figure 12, was held onboard the boat. When the source was submerged to the desired depth, the plunger would be thrown down the line, breaking the lightbulb. The bursting of the lightbulb and the ensuing movement of water was able to produce a sound of great enough amplitude to be detected from a source kilometers away. A standalone depiction of the lightbulb apparatus is shown in Figure 13.

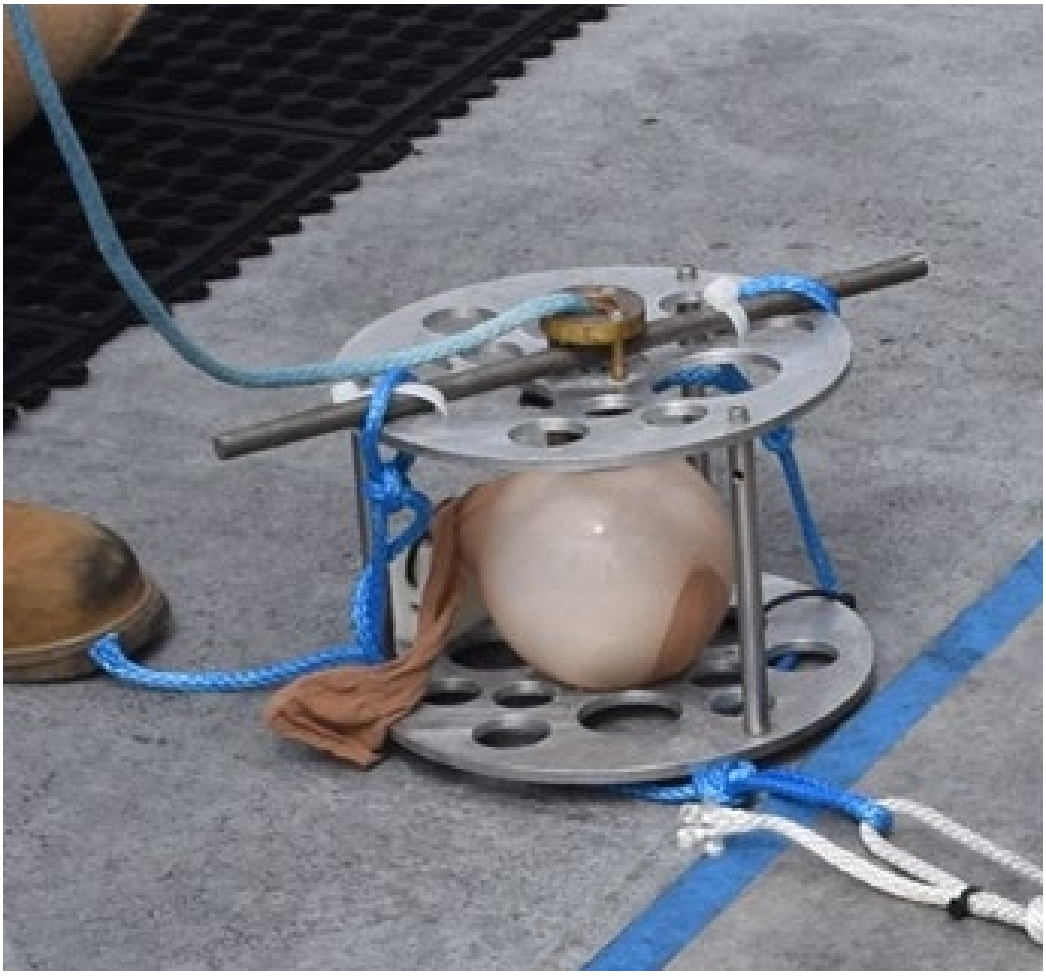

Figure 13. Imploding lightbulb source

To counteract the buoyancy force of the balloons, sandbags were created by filling burlap bags with sand. Originally, when four balloons of 18 inch diameters were planned to be used, the necessary weight was calculated to be 450 pounds. However, as the volume of the balloons used ended up being lesser than originally intended, the value necessary for weighting is unknown. The weighting system is shown in Figure 12 in the rightmost burlap bags.

The receivers used for the experiment included an icListen hydrophone tied off roughly 21 meters from the source as well a bottom mounted GTI M20-105 vector sensor. The vector sensor was located at coordinates of 36.904 N and 122.203 W in roughly 98 meters of water. Upon observation of the data, the data collected from the icListen was very noisy and it was difficult to distinguish the implosion of the lightbulb from the noise.

3. Procedure

In conducting the experiment, we began drifting away from the receiver around 1130 and roughly 6 kilometers from the receiver. While drifting, we lowered the apparatus to a depth of 10 meters, which was marked by a change in color on the line. Once the depth was reached, we would turn the engine of the boat off to minimize self-noise. At this point, the plunger was propelled downward to burst the lightbulb. Once the burst was confirmed, the apparatus was raised back on the deck and the burlap bag with the balloons was removed and the lightbulb was replaced. The same process was then repeated without the balloon. At the time of each burst, the location, time, and set up (with or without balloon) were recorded in a logbook.

Once this procedure was repeated three times, each with and without the balloon, the same process was attempted at a depth of thirty meters. However, issues arose at thirty meters as the line became tangled, which did not allow for the bursting of the lightbulb. Additionally, it became clear after a number of failed attempts that the balloons had burst inside the burlap bag at some point during the experiment. Although the balloons had burst, the plastic bag they were in remained partially inflated, so it is uncertain at what point the balloons popped.

B. DATA ANALYSIS

The first step in processing the data collected from the bottom mounted vector sensor was to simply look for general trends in the data. The magnitude of the normalized, uncalibrated pressure measurements was plotted over the thirty-minute window of interest during the testing conducted with the source at a depth of ten meters. The data was plotted both in terms of the normalized pressure as well as the decibel scale, as shown in Figure 14. It is important to note that Figure 14 is simply a comparison of the raw, uncalibrated data collected by the receiver. The plot shows a clear decrease in magnitude over the broadband frequency content of the bursts. The relative pressure ratio and decibel reduction over the three trials and on average are shown in Table 3. Based on the broadband comparison between the burst with and without a balloon the bursts with the balloon show a distinct reduction in sound.

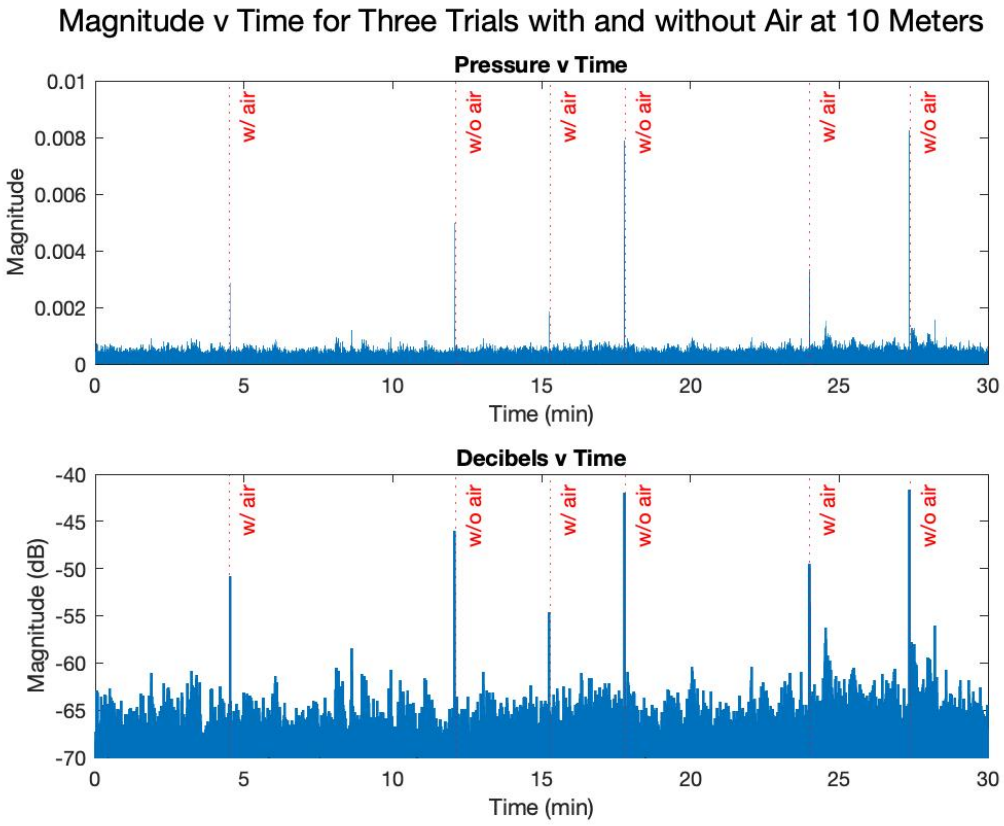

Figure 14. Plot of magnitude over time

Table 3. Pressure and decibel reduction of bursts

	TRIAL 1	TRIAL 2	TRIAL 3	AVERAGE
PRESSURE RATIO (P/P_0)	0.5744	0.2357	0.4165	0.4089
DECIBEL REDUCTION (DB)	4.8160	12.5520	7.8390	8.4023

In order to represent the data in the form of proper units, the received data had to be properly calibrated. Using the calibration curve for the receiver, shown in Figure 15, the data points were multiplied by the corresponding calibration value for the frequency of the point. This process allowed for the pressure values to be represented in terms of Pascals.

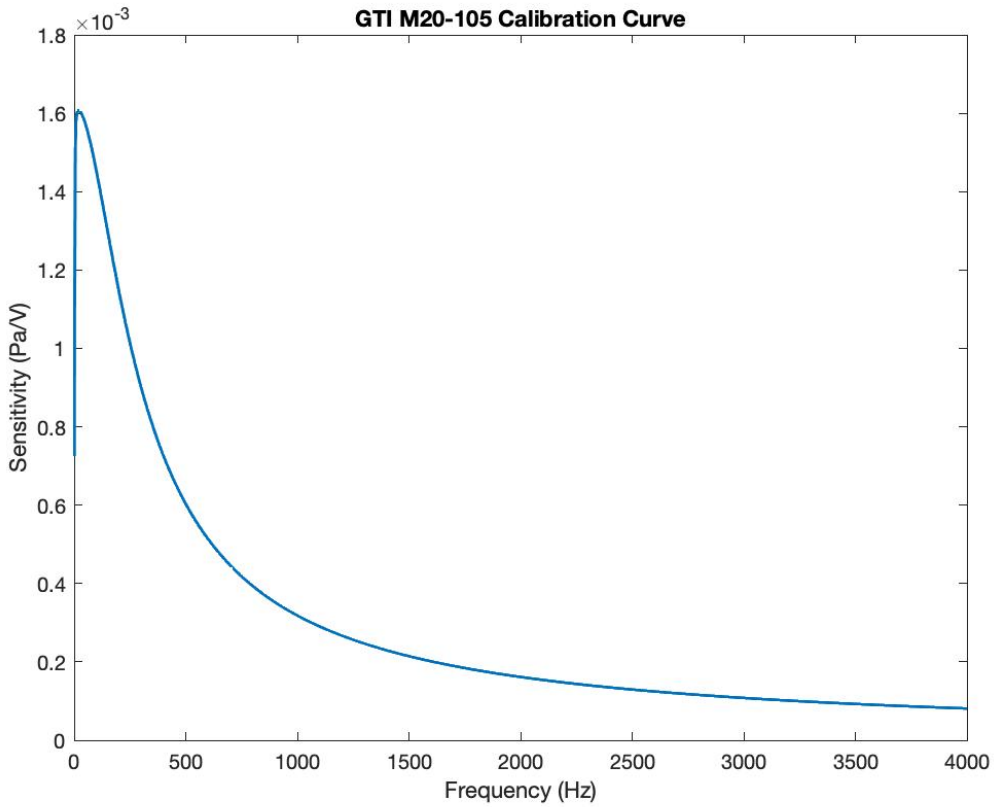

Figure 15. Calibration curve for receiver (GTI M20-105)

After calibrating the data, the next step was to generate the spectra of the signals. Using the audio editing software Audacity [12], the frequency content and length of a lightbulb burst was determined. Each burst conducted at ten meters was then isolated and extracted to allow for more efficient manipulation. The frequency content of the bursts was determined to be up to roughly 600 Hz and the length of the signal was taken as approximately 0.6 seconds. The fast Fourier transform of each isolated burst was taken in order to transform the data into the frequency domain. Once the time domain data was converted into the frequency domain, the amplitude of the signal pairs (with and without the balloon) were plotted together for comparison, shown in Figure 16. To make the trends in the data more apparent, a moving average was determined for each of the signals using a moving window of 10 Hz, 20 Hz, and 40 Hz for the frequency ranges of 0–100 Hz, 100–200 Hz, and 200+ Hz, respectively. To properly average the data, the intensity at each point was calculated from the pressure. Next the intensity vector was averaged and converted back to pressure and plotted. The averaged spectra of the signals is shown in Figure 17.

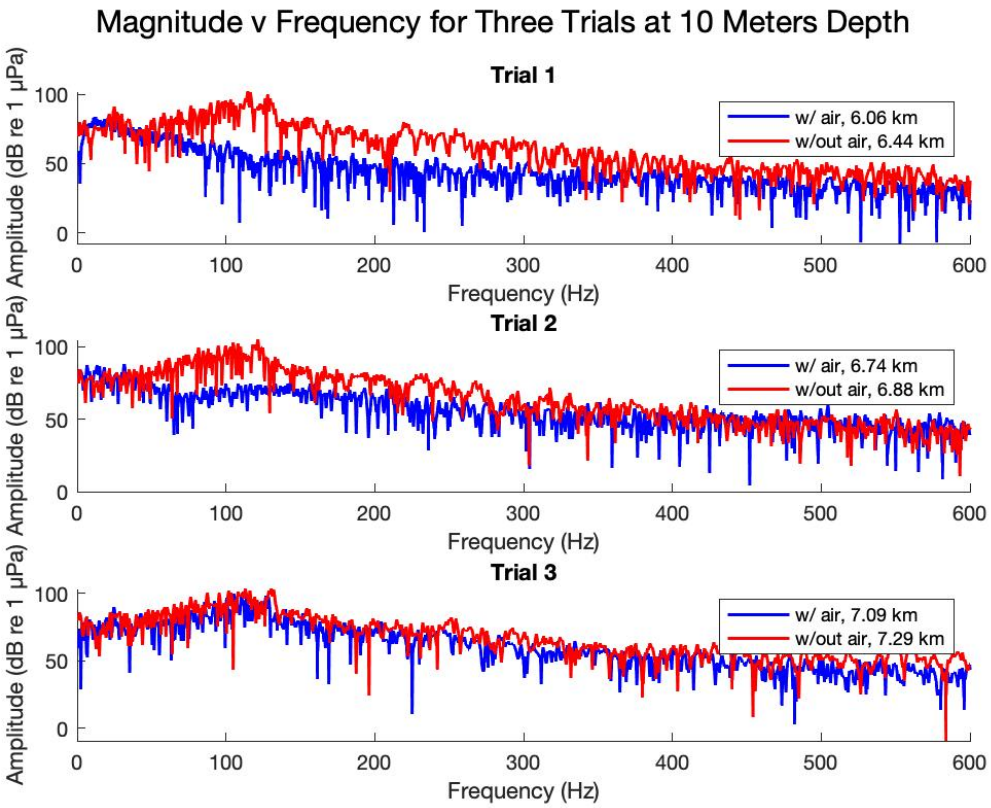

Figure 16. Spectra of signals with and without balloon

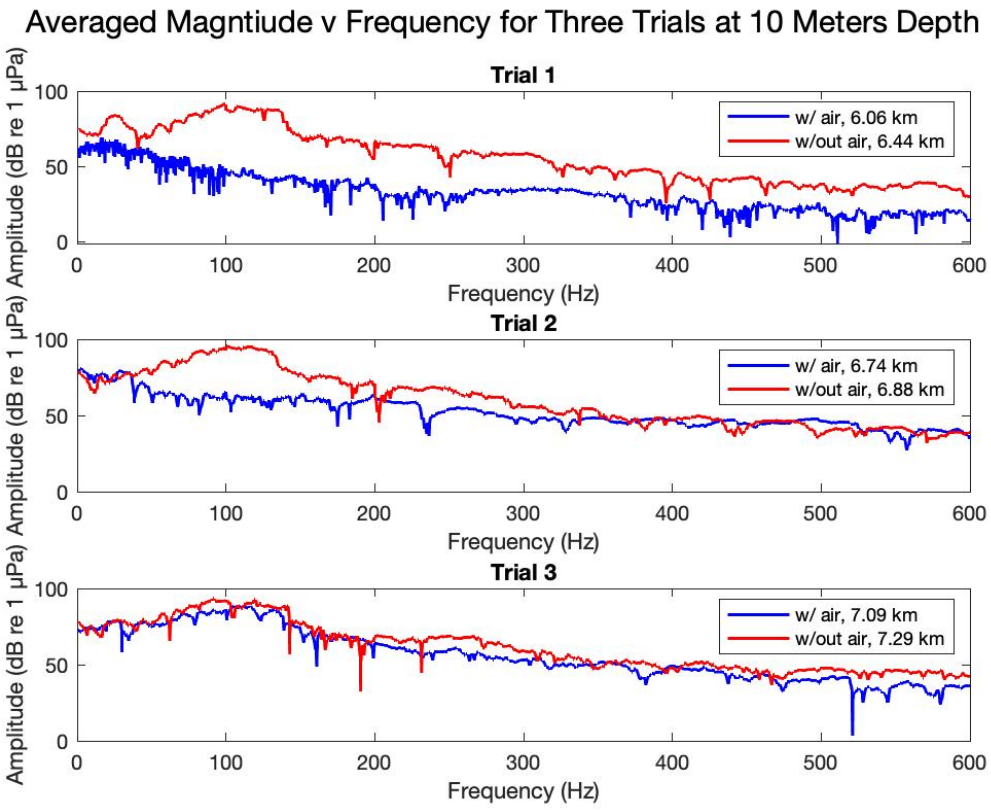

Figure 17. Averaged spectra of signals with and without the balloon

The spectra of the signals indicated a very clear trend in suppression throughout most of the frequency range. In all three trials, it is quite clear that the amplitude without the air was consistently greater than that of the signals with the balloons present. However, despite there being a consistent general trend, there is inconsistency between the three trials as trial one and two show significantly greater suppression than that of the third trial. Trial three differs as it holds a relatively constant value of suppression along the entire frequency content where the first two trials indicate much greater suppression at the lower frequencies, as supported by the theory. Based upon the minimal suppression present in trial three, it was deemed likely that the balloons had burst at this point and there was only a small amount of air remaining in the bladder.

It was also desirable to examine the ambient noise around the time of each burst. In order to properly assess the noise, a roughly one second window of the recorded data

was isolated from the time immediately after the burst subsides and before the engine of the boat was turned back on. The same process used to create the spectra of the signals was used to generate the spectra of the noise, shown in Figure 18. In the same manner as with the burst signal, the noise spectra were smoothed using the same moving average frequency band, shown in Figure 19.

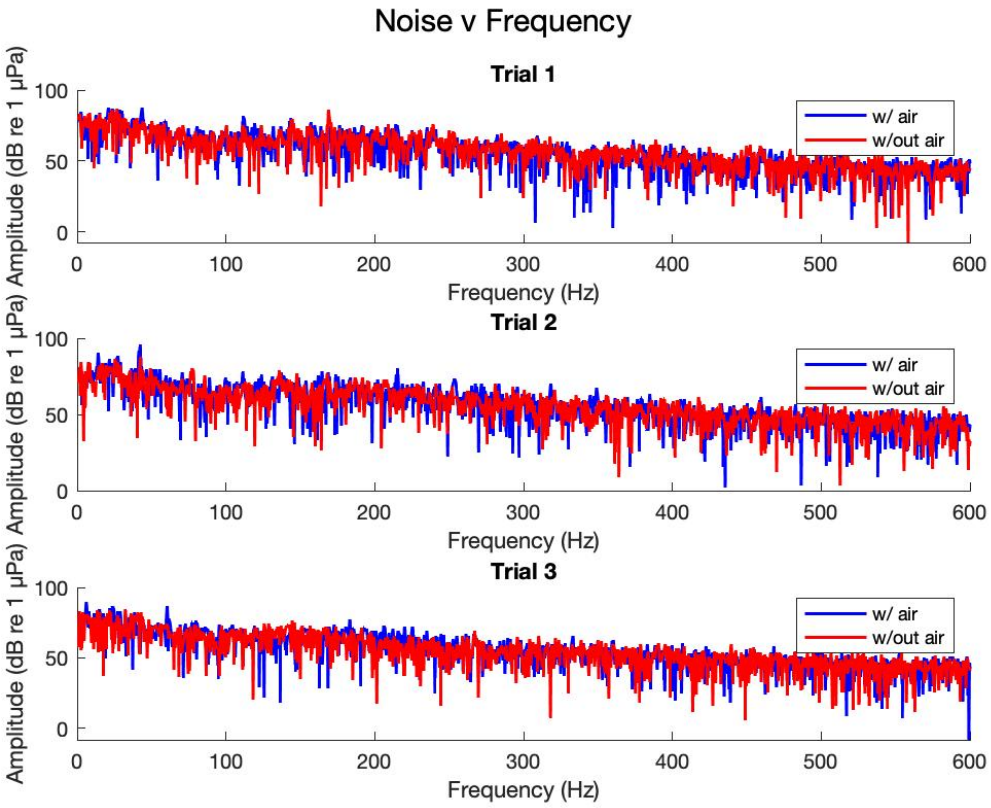

Figure 18. Noise spectra in bay

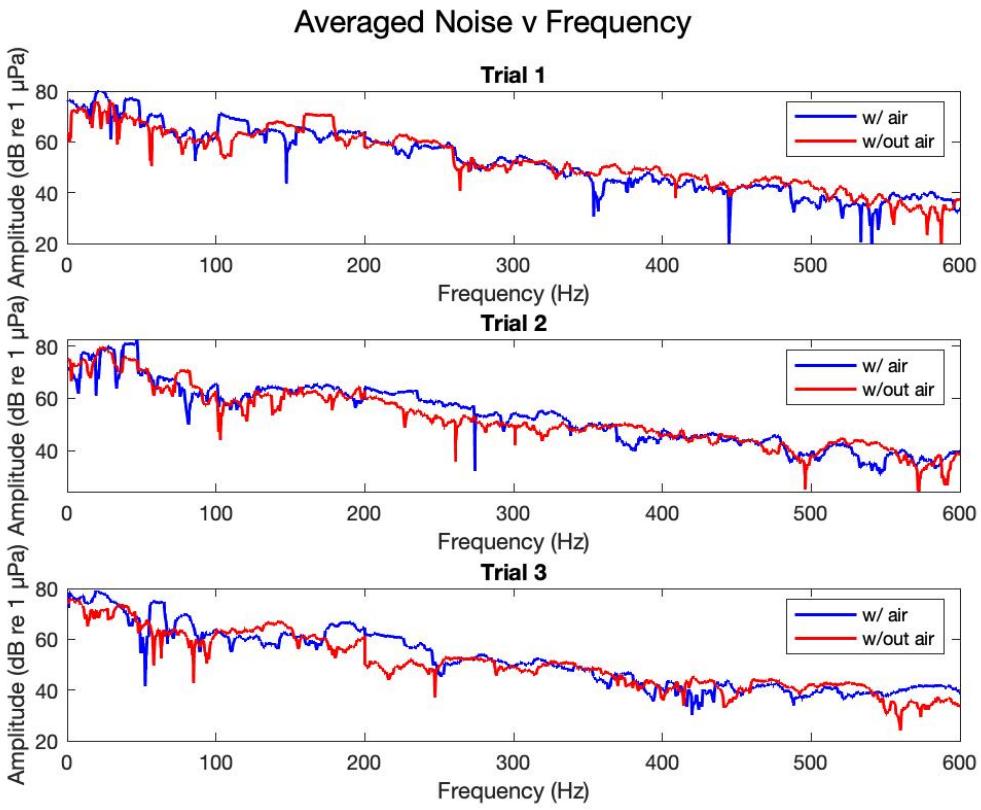

Figure 19. Averaged noise spectra

The noise spectra provided useful insight into the behavior of the lightbulb burst signals. The noise is shown to be relatively similar among the frequency range for each of the three trials, indicating that no single trial or burst had any significant increase or decreased in background noise, although there are some slight variations. Additionally, it can be concluded that the suppression indicated by the spectra of the signals is not due to any changes in the ambient noise. Similarly, there is no clear trend between the noise samples taken after the burst with or without the balloons. This agrees with the theory as the presence of the balloons should not have any impact on the ambient noise recorded by the receiver. Furthermore, in comparing the noise spectrum to that of trial three, there are notably similarities in the shapes of the curve, reinforcing the idea that the balloons, or at least one balloon had indeed popped by this trial.

In order to further explore the trends in the data, the variability in the signal and noise was compared to the effect of the balloon. In order to determine the variability of the signal, the absolute value of the difference in the signal vectors were plotted over the frequency range. This was conducted for the three sample with and without the balloons. For example, the difference in the signal from trial one with the balloons and that from trial two with the balloon was taken. This was repeated for trial one and three and trial two and three. The same process was used for the signals without the balloons. For the noise, the difference was taken in the same manner as the signal in order to show variability of noise between trials. Additionally, the difference in noise recordings collected from the same trial was taken for each trial. Finally, the effect of the balloons was determined by taking the difference in the signal with and without the balloons for each trial. The results are shown in Figure 20. As shown, there is a considerable amount of variability between the trials, especially apparent in the signals without the balloons. However, it must be considered that the separate trials were conducted under different conditions (distance to receiver for example). Overall, despite significant variation in the signal, the variation is not greater than the effect of suppression generated by the balloons.

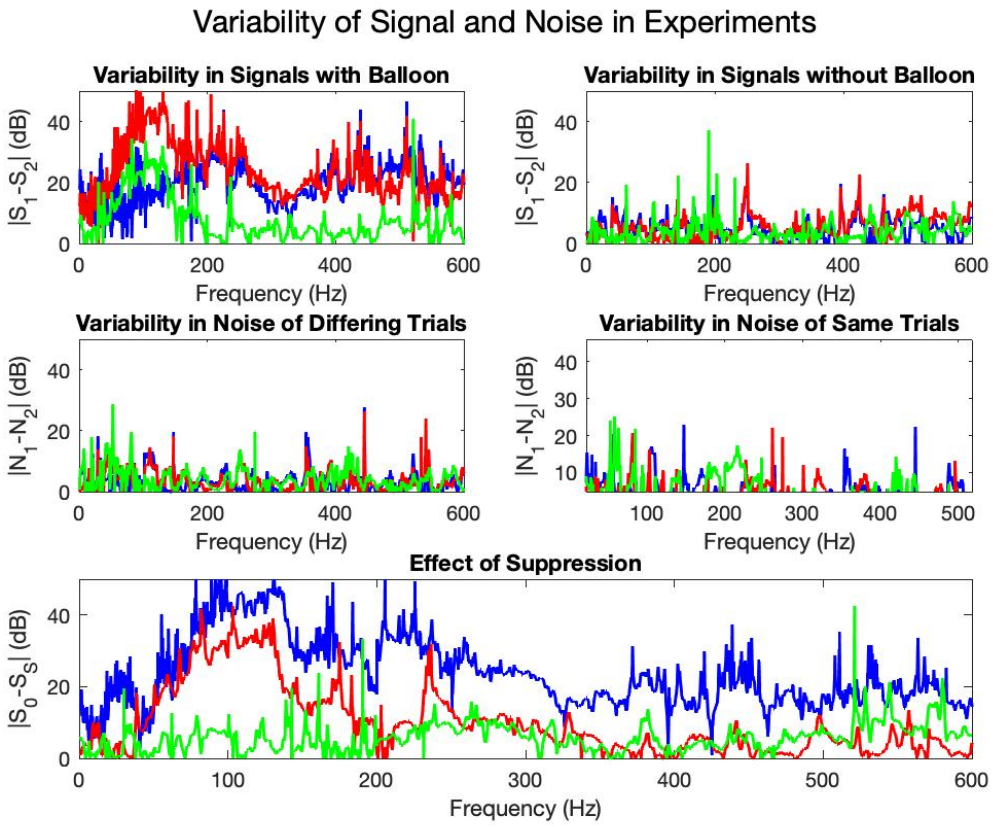

Figure 20. Variability in signal and noise

Finally, it was desirable to examine the decibel reduction of each of the three trials. In order to calculate the reduction, the averaged values of the amplitude of the signals were used. The averaged vector with the balloon was subtracted from the averaged vector without the balloon and plotted over the frequency range for each trial, as shown in Figure 21.

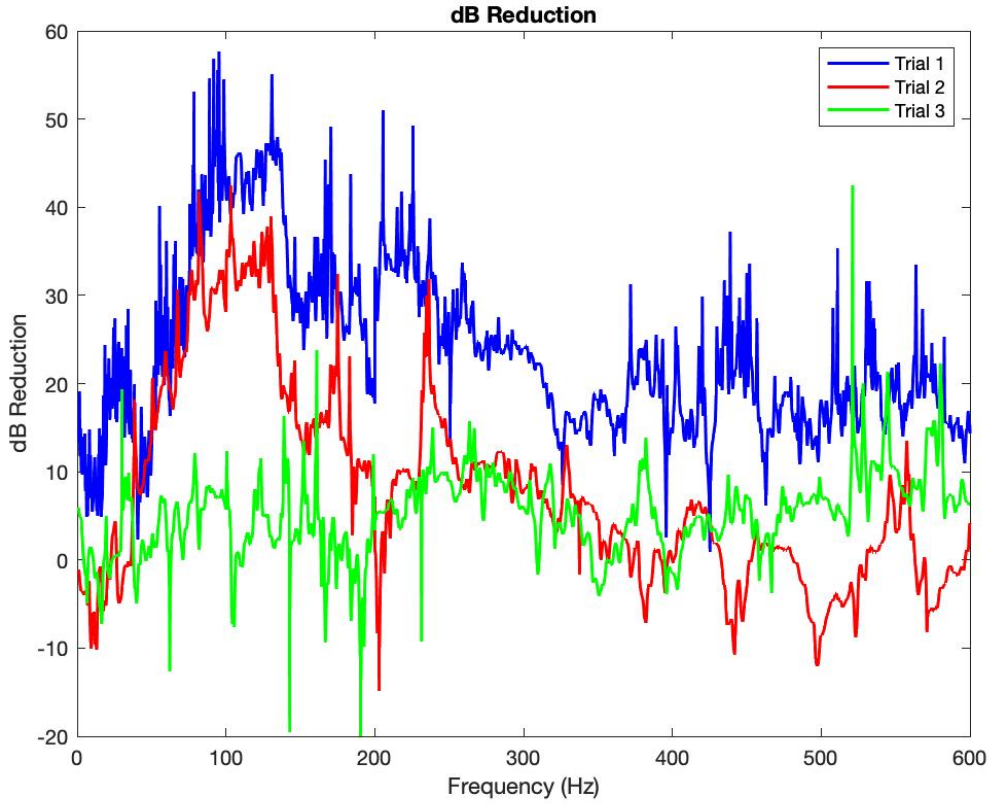

Figure 21. Decibel reduction over frequency

As noted from the spectra of the signals, the same clear trend exists as there is notable reduction in all three trials. Additionally, the same inconsistency with trial three persists, while trial one and trial two hold roughly the same shape. As shown in Figure 21, trial one shows a maximum reduction of roughly 55 decibels. The maximum of trial two occurs at roughly 35 decibels. Also notable is that while trial two has a lesser reduction in sound, the peaks seem to arrive at a slightly lower frequency value than seen in trial one. In order to better understand the results, comparison to theoretical models was necessary.

C. COMPARISON TO THEORETICAL MODELS

Using a similar method as was used for the Spanagel Hall tank experiments (Chapter II), the experimental pressure ratio was compared to the values given by theoretical model. Due to the significant uncertainty in the value of the parameters (e.g.: radius, a) in the bay experiment, a range of parameters had to be estimated. The low end of the estimates include

the values that would produce the lowest suppression values while remaining within the range of reason in parameter estimation. Similarly, the high end is comprised of the values that would create the highest amount of suppression. The values estimated and used in calculating the theoretical pressure ratio are given in Table 4. The resulting comparison of the experimental and theoretical pressure ratio are shown in Figure 22.

Table 4. Parameters used to calculate theoretical pressure ratio for bay experiment

Trial – Low/High	*a (m)*	*b (m)*	*R (m)*	*M*	*s*
Trial 1 – Low	0.225	0.53	6060	0.025	$2/9(1+0.01i)$
Trial 1 – High	0.600	0.65	6440	0.013	$2/9(1+0.01i)$
Trial 2 – Low	0.225	0.53	6740	0.025	$2/9(1+0.01i)$
Trial 2 – High	0.600	0.65	6880	0.013	$2/9(1+0.01i)$
Trial 3 – Low	0.225	0.53	7090	0.025	$2/9(1+0.01i)$
Trial 3 - High	0.600	0.65	7290	0.013	$2/9(1+0.01i)$

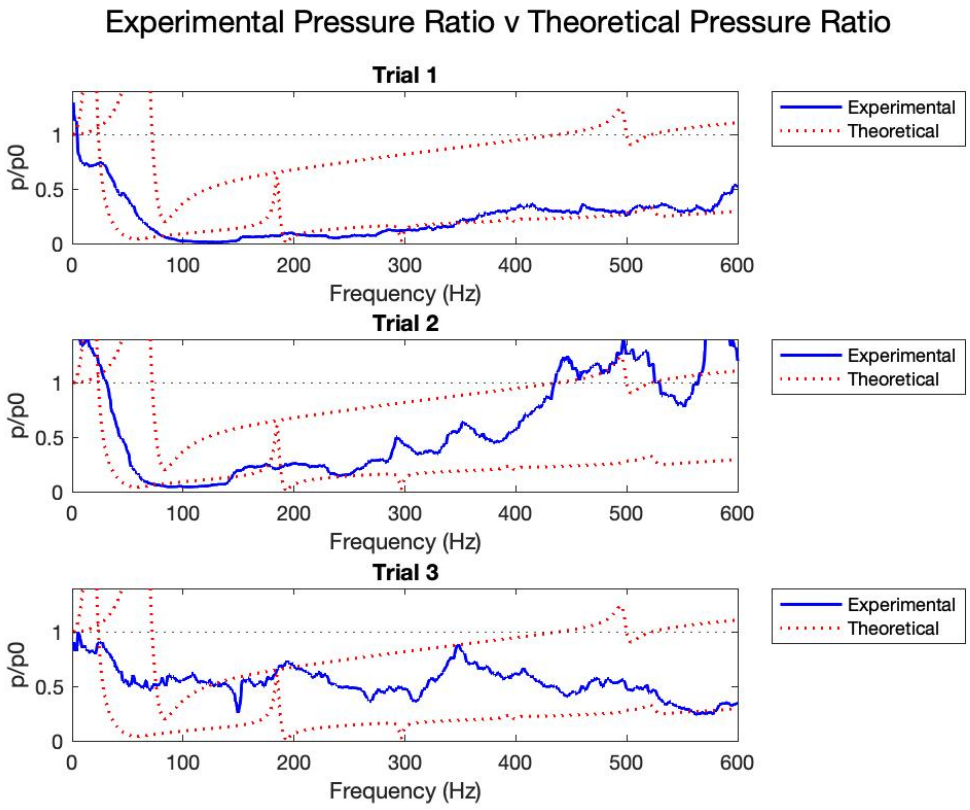

Figure 22. Pressure ratio versus frequency for bay trials

Despite the wide range of uncertainty within the experimental parameter, the experimental and theoretical pressure ratio show relative agreement. Trial one shows reasonable agreement with the higher end of suppression as it peaks at roughly the same frequency and follows the general slope. Trial two seems to agree with the higher end of suppression up to 300 Hz where it begins to show resemblance to the lower end of the theoretical curve. Trial three does not resemble either bound, however, it does fall within the projected range of suppression for much of the frequency range. Also noteworthy is the agreement in the theory and the experimental data that there is a small band of frequencies in the very low range that can show a slight amplification of the signal.

To best compare the data to the theory, it was important that more known factors were implemented into theoretic modeling. The previously used models assumed a spherical air bladder—which is clearly not the case—and open space. An advanced

mathematical model of sound suppression has been developed to take into account the effect of the ocean surface on the acoustic field. In the absence of the scatterer acoustic field consists of a direct wave from the source and surface reflection. When a compliant object (an air bladder) is placed near the source, the advanced model of the acoustic field consists of three components: (a) the direct wave from the source and the wave scattered by the object (as in the unbounded medium), (b) reflections of the direct and the scattered wave from the ocean surface, and (c) the additional scattered wave, which is generated when the reflected waves are incident on the object. It can be demonstrated that higher-order multiple scattering is negligible in the geometry of the experiment as long as the dimensions of the object and the distance from the source to the object are small compared to the source depth. The model predicts dependence of the resulting acoustic field on the depth of the source, D, the depth of the receiver, z, and the position of the source relative to the object. The model assumes a spherical object, and the position of the source is characterized by the angle Ψ between the directions vertically upward and to the source from the center of the sphere. Because the air bladder was far from spherical in the field experiment, only semi-quantitative agreement between measurements and the model can be expected.

Using this advanced model, similar plots to that shown in Figure 21 were generated while altering the parameters a and Ψ. The baseline parameters used in this modeling are included in Table 5. Figure 23 shows the decibel reduction across the frequency range for three different values of the radius. When compared to Figure 21, it is evident that there are significant similarities between the theory and the first two trials. The most noticeable is peak of suppression around roughly 100 Hz. In the experiments we recorded a reduction of roughly 35–50 decibels at this peak which agrees with the predictions provided by the theory. It is also worth noting that the theoretical curve for a radius of 0.2 meters is quite smooth, resembling the trend of trial three, which likely had a decreased volume of air. However, despite similarities, there are still clear disagreements between the theory and experimental results (as expected), most notably involving trial three.

Table 5. Parameters for advanced modeling

a (m)	D (m)	z (m)	R (m)	Ψ (rad)	M	s
0.6	10	100	7000	0	0.013	$2/9(1+0.01i)$

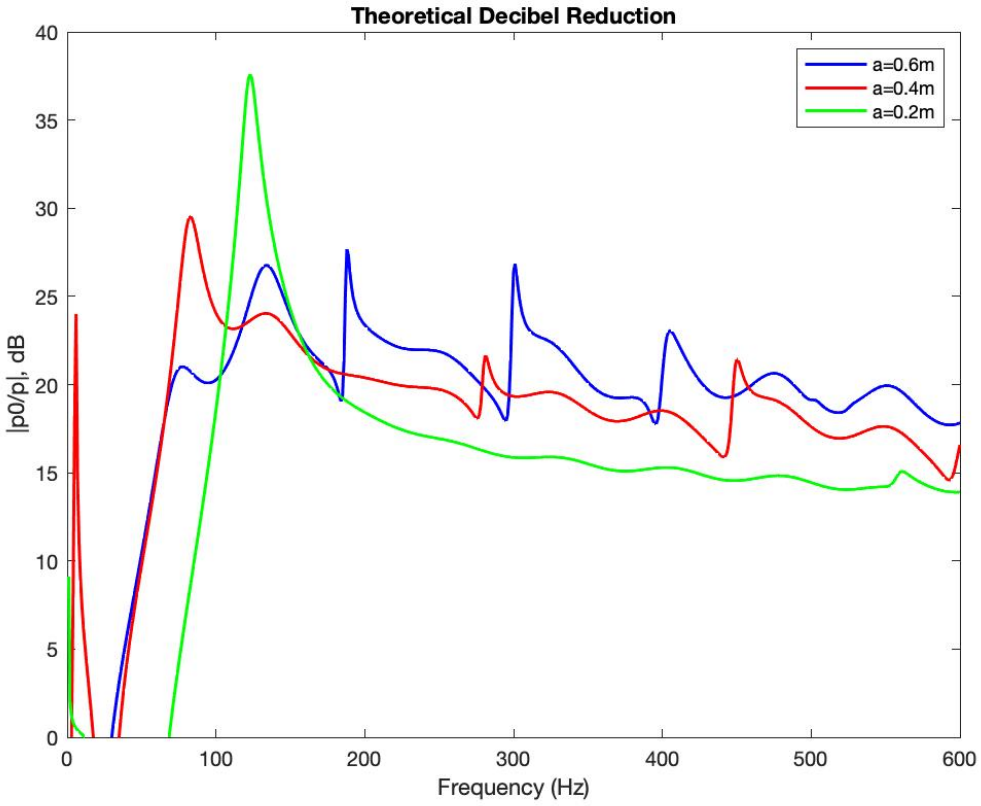

Figure 23. Theoretical suppression for various values of a

One way to explain the disagreement between the models and experimental results is simply the lack of accurate parameters. Furthermore, this would be compounded by the ocean bringing into question a number of additional unknowns. For example, although the bag holding the balloons was tied to the source, there is no way of knowing what the angle, Ψ was or what the distance between the source and the balloon was at the time of implosion. This is significant as there are considerable variations in the predicted suppression depending on what the value of Ψ is taken as. Figure 24 shows the theoretical predictions for a base radius of 0.6 meters and various values of Ψ.

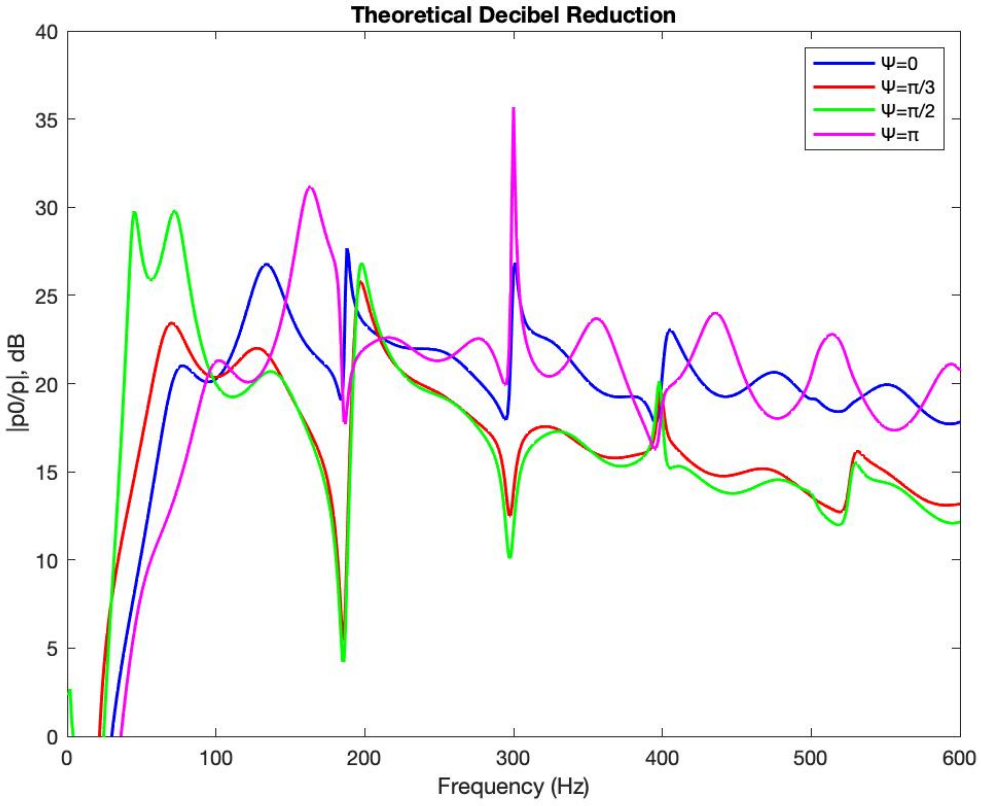

Figure 24. Theoretical suppression for various values of Ψ

As shown in Figure 24, there is considerable change in the shape and magnitude of the theoretical suppression curve based on the changing of the angle, Ψ. It is reasonable to expect that as the experiment was occurring, this angle could have changed as the balloons drifted or as they were tied on to a different location. Such as change could have impacted the results significantly. Along with changes in the angle, it is also reasonable to expect that the distance between the source and the balloon, *b*-*a*, likely changed during the experiment, be it during one trial or between trials. Such changes in parameters would have significantly impacted the accuracy of our theoretical models. Additionally, modeled assumptions such as the air bladder being a sphere did not translate into the experiment, further increasing the error between the models and experimental results. Finally, there is the issue of the popped balloons. Since the balloons were wrapped in a plastic bag, there would have still been air inside while at depth, even if the balloons popped. However, the

volume of air in the bag was considerably less due to there being relief holes in the plastic bag. It is not unreasonable to think that the balloons burst prior to trial three, creating a smaller radius of air and a greater distance from the source. This could give trial three lesser reduction and as shown in Figure 23, a flatter curve. When combined with other unknowns throughout the experiment, it is possible that this allowed for the deviations seen in trial three. It is also significant to note that in both Figure 23 and Figure 24, significant suppression is still predicted, even towards the higher end of the frequency content. Based upon the models, this is expected to continue up to values of at least 1000 Hz, although our examined frequency range was much narrower.

IV. CONCLUSIONS AND FUTURE WORK

A. SPANAGEL HALL EXPERIMENTS

Our controlled experiments in the Spanagel Hall tank indicated that there is very likely a correlation between the presence of an air bladder and the suppression of underwater sound. However, the trends in the experimental data are not sufficiently certain to draw concrete conclusions due to limitations thought to be brought upon by the tank. The relatively small size of the tank allows for reflections to interfere with the experiments on the scale we conducted, therefore complicating the results and making the comparison with theory difficult. Despite this, when accounting for the very fundamental differences in parameters between the models and experiments, the agreement shown from our testing is significant. This being said, controlled experiments should be conducted in a significantly larger tank in order to best enable the comparison to theory and to allow for the suppression effect to be studied effectively.

The NPS SLAMR tank is a logical next step in the experimental process as it provides a sufficient increase in size to conduct effective experimentation. The improvements made in the Spanagel tank lab in this thesis allow for the transition to the SLAMR tank. The improved anchor (Section II.C) allows for a larger sphere to be used, which is essential in taking advantage of the dimensions of the SLAMR tank. Additionally, the improved source, the ITC-1042 (Section II.A), would allow for an optimal geometry for experiments in the larger tank, while not being too small for the increased scale. Additionally, the improvements in the experimental process (Section II.D) will allow for data to be taken much more efficiently, which will be advantageous in overcoming the difficulties in transitioning to the SLAMR facility.

Although the SLAMR facility provides a logical next step in the future of controlled sound suppression experimentation, the ultimate goal should be to eventually work in a much larger facility. One such facility is the Transducer Evaluation Center or TRANSDEC facility located in San Diego, California, pictured in Figure 25. The TRANSDEC facility is 38 feet deep with dimensions of 300 feet and 200 feet in the shape of an ellipse. The

facility is used for transducer calibration which provides the benefits of it being easily accessible for equipment, anechoic, having low ambient noise, and simulating open ocean properties [13]. Of course, such a facility would introduce its own unique challenges—most obvious being cost and travel, but if future work allows for such access, it would create invaluable opportunities to explore ocean-like applications of the theory in a controlled environment.

Figure 25. TRANSDEC facility. Source: [13].

B. EXPERIMENTS IN MONTEREY BAY

Although rough, the experiment conducted in Monterey Bay provided very fruitful results. Throughout all three of the trials at ten meters in depth, significant suppression was demonstrated over the frequency content of the lightbulb burst. There was significant agreement in the shape and magnitude of the experimental data and the theoretical curves as well. Despite some minor disagreements between the theory and the experimental results, there is strong evidence supporting that the broad band sound suppression effect was occurring in our experiments. This is further supported when considering the conditions in the bay were not fully accounted for in the theoretical models used and the models were only designed as a qualitative comparison.

The next step should be to conduct more testing in Monterey Bay or elsewhere in the ocean. When conducting future experiments, it is critical that the experimental process be refined in order to maintain better accuracy in the input of experimental parameters for theoretical models. As indicated by this thesis, the theoretical models can and should continue to be incorporated with more refined experiments to best understand the theory and its valuable applications. It will also be desirable to conduct testing at numerous and deeper depths. Another improvement that should be made in future testing is to employ data from multiple receivers, allowing for the verification of results such as those seen in trial three.

THIS PAGE INTENTIONALLY LEFT BLANK

LIST OF REFERENCES

[1] O. A. Godin and A. B. Baynes, "Passive, broadband suppression of low-frequency sound," *Journal of the Acoustic Society of America,* vol. 143, no. 2, pp. 67–73, 2018.

[2] E. McMellon, "Observation of Passive Broadband Suppression of Low-Frequency Underwater Sound," M.S. thesis, Department of Physics, Naval Postgraduate School, Monterey, CA, 2020.

[3] "Assembled Sensors and Transducers," CeramTec, 2021. [Online]. Available: https://www.ceramtec-industrial.com/en/industries/piezo-applications/assembled-sensors-and-transducers. [Accessed 2021].

[4] "Piezoelectric Ceramic Products," Piezo Kinetics Incorperated, 2021. [Online]. Available: https://piezo-kinetics.com/piezoelectric_ceramic_products/. [Accessed 2021].

[5] "Products and Solutions," Data Physics, 2021. [Online]. Available: https://www.dataphysics.com/products-and-solutions/signalsound-high-intensity-and-underwater-acoustics.html.

[6] "Underwater Acoustic Modems," Evo Logics, 2021. [Online]. Available: https://evologics.de/acoustic-modems#midrange. [Accessed 2021].

[7] International Transducer Corporation, Santa Barbara, CA, model 1042.

[8] O. B. Wilson, Introduction to the Theory and Design of Sonar Transducers, Los Altos, CA: Peninsula Publishing, 1991.

[9] Giraffe Manufacturing, "Punch Balloons," Mesa, AZ, 2021.

[10] Mathworks, "MATLAB 2021a." Natick, MA 2021. Available: https://www.mathworks.com/products/matlab.html.

[11] Wolfram, "Mathematica 12.3." Champaign, IL 2021. Available: https://www.wolfram.com/mathematica/?source=nav

[12] The Audacity Team, "Audacity." 2021. Available: https://www.audacityteam.org/download/.

[13] Federal Labratory Consortium, “Transducer Evaluation Center (TRANSDEC),” FLC, 2021. [Online]. Available: https://federallabs.org/labs/transducer-evaluation-center-transdec#about. [Accessed 2021].

INITIAL DISTRIBUTION LIST

1. Defense Technical Information Center
   Ft. Belvoir, Virginia

2. Dudley Knox Library
   Naval Postgraduate School
   Monterey, California